IEEE Access
Multidisciplinary ⋮ Rapid Review ⋮ Open Access Journal

Received March 24, 2017, accepted April 8, 2017, date of publication April 25, 2017, date of current version February 28, 2018.

Digital Object Identifier 10.1109/ACCESS.2017.2697867

Guided-Wave Properties of Mode-Selective Transmission Line

FAEZEH FESHARAKI[1,2], TAREK DJERAFI[3], MOHAMED CHAKER[4], AND KE WU[1], (Fellow, IEEE)

[1]Poly-Grames Research Center, Ecole Polytechnique de Montreal, Montreal, QC H3T 1J4, Canada
[2]Department of Electrical Engineering, University of Victoria, Victoria, BC V8P 5C2, Canada
[3]INRS-EMT, Montréal, QC H5A 1K6, Canada
[4]INRS-EMT, Varennes, QC J3X 1S2, Canada

Corresponding author: Faezeh Fesharaki (faezeh.fesharaki@polymtl.ca)

This work was supported in part by the NSERC and in part by the Canada Research Chair Program.

ABSTRACT The so-called mode-selective transmission line or simply ''MSTL'' is studied theoretically and experimentally. This low-loss and low-dispersion transmission line operates with a frequency-dependent mode-switching behavior. This self-adaptive mode-selective guided-wave structure begins with the propagation of electromagnetic waves over the lower frequency range in the form of a quasi-TEM fundamental mode similar to the microstrip line case, then followed by a fundamental quasi-TE_{10} mode with reference to rectangular waveguide over the higher frequency region. To gain insight into the physical mechanism and fundamental features of this mode-selective transmission line, a detailed semi-analytical hybrid-mode analysis is developed through the application of a method of lines. This method allows accurate and effective modeling of MSTL guided-wave properties. Propagation characteristics of this proposed mode-agile structure in terms of dispersion, modal, and loss properties are examined, which leads to the establishment of some basic MSTL design guidelines. Numerical results confirm the expected mode conversion and low-loss behavior through the observation of field evolutions along the structure. For experimental verification, a set of MSTL prototypes are fabricated on two different substrates through dissimilar fabrication processes. Measurements are carried out from dc-to-500 GHz using a vector network analyzer. Excellent agreement between theoretical and experimental results is observed. It is confirmed that the low-dispersion and low-loss behavior of MSTL makes it an outstanding integrated waveguide in support of high-performance super-broadband signal transmission and/or ultra-fast pulse propagation in a fully-integrated platform.

INDEX TERMS Mode-selective transmission lines (MSTL), hybrid mode analysis, method of lines (MoL), super-broadband signal, ultra-fast pulse.

I. INTRODUCTION

A. GENERAL

Electromagnetic (EM) waveguiding techniques have been established as one of the earliest milestone developments in radiofrequency (RF), wireless, and microwave engineering. They have been truly instrumental as any successful and practical design and application of high-frequency electromagnetic devices, circuits, and systems, are closely related to the deployment of their distinctive guided-wave properties. Although rectangular waveguide has been in use since the 1930s, the intensive development of microstrip line and coplanar waveguide, which started, respectively, in the 1950s and 1960s, has been considered as the most critical driving force for the design of RF and microwave integrated circuits and systems. Integrated transmission lines in the form of microstrip, coplanar waveguide, and their derivatives of geometry have been the backbone of the modern electronic and photonic integrated circuits and systems. Following the evolution of ICs technologies and processing techniques in the field, those fundamental structures have been continuously studied and improved to meet the constantly updated bandwidth and expanded capabilities requirements. However, the ever-increasing demands for bandwidth and performance as well as the highly anticipated applications of millimeter-wave (mmW) and terahertz (THz), have raised the fundamental question of whether those classical transmission lines are able to cope with the demands for low-loss and low-dispersion guided-wave propagation [1]. Indeed, planar transmission lines are the foundation of any high-frequency ICs, such as RFICs and MMICs, whose performance factors and

cost indices are first limited by the transmission line building elements.

Currently, the increase in bandwidth related to ultra-high-speed wireline digital domains or computing systems such as memory chips, CPUs, GPUs, backplanes, and wired LANs, are enabled by increasing the number of input/output (I/O) channel interconnects on chips [1].

To keep up with bandwidth demand and to avoid prohibitive cost and complexity, fast time-domain pulse signals would require bus lines or interconnects design to support low-loss and low-dispersion signal transmission from dc to mmW spectrum, and even up to THz bands if pico-pulsed signals are used. In this case, each set of existing I/O channels would be replaced by a single ultra-wideband interconnect. On the other hand, in wireless application, although radio-over-fiber techniques are applied and complicated modulation schemes are used, available RF bandwidth is still relatively low [2]. In this case, the challenges are in pushing the use of RF signals toward the frequency range of mmW and higher, which necessitates the development of ultra-high-speed electro-optical devices such as modulators and photodetectors for which high-performance dc-to-mmW/THz ''electronic'' transmission lines are needed for integrated ''electrodes'' [3].

Efficient guiding of electromagnetic waves through analog interconnects with minimized dispersion and loss effects over an extended bandwidth on a chip is of paramount importance for future broadband front-ends in wireless systems [4], [5]. The fact is that using transmission lines operating up to mmW/THz frequency range is a long-term solution to providing outstanding large bandwidth with minimum cost and complexity in both wireline/wireless and digital/analog applications. The system-on-chip concept [7], [8], which is being extended from RF and microwave applications to mmW and THz integrated platforms, critically depends on the use of transmission line and chip-interconnect properties. Obviously, worldwide efforts have been made for a long time to evolve and improve the existing transmission line structures through numerous incremental manners, but it still remains an ultimate scientific and technological challenge, which necessitates the emergence of a revolutionary concept.

B. THEORETICAL BACKGROUND

Depending on waveguide structure, guided waves exhibit different operating modes in the frequency domain, featuring different loss and dispersion behaviors. The microstrip line supports a fundamental quasi-TEM mode in which longitudinal field components along the propagating direction are negligible compared to their transverse counterparts. Its signal line presents a longitudinal current distribution changing from a minimum in the middle to an over-shoot (singularity) at the two line edges. As frequency goes higher and higher, the current becomes more and more confined to the surface, resulting in increased resistance and, therefore, skin effects are much more pronounced. Note that the substrate thickness and line width are generally reduced as frequency increases to comply with the impedance design. As a result, TEM mode-related conductor or ohmic losses increase with frequency. TEM mode has no cut-off frequency but at higher frequency, other modes begin to propagate on a microstrip line, resulting in excessive dispersion effects beyond a certain frequency point. Therefore, this transmission line is not amenable to the mmW/THz frequency range because of some prohibitive signal attenuation coupled with modal dispersion.

An emerging planar technology called substrate integrated circuits (SICs) has recently been studied and developed for various microwave and millimeter-wave applications [9], [11]. This scheme allows for the making of any non-planar structures in planar form, which renders possible the synthesis and integration of rectangular waveguide, dielectric waveguides, and coaxial lines at low cost with high performance. Among the proposed SICs topologies, easy-to-make planar synthesized rectangular waveguide or substrate integrated waveguide (SIW) has been the most popular, which supports the fundamental quasi-TE mode [12]. Having a longitudinal component of magnetic field along the propagating direction, the TE mode (mainly TE_{10} mode) can be decomposed into two plane waves according to the waveguide theory, which bounce back and forth between the waveguide sidewalls with s-polarized incidence while propagating. The electric field fades on the metallic surfaces, and losses of the TE mode follow a steady unchanging trend with increasing frequency [13], [14].

In 1970 at Bell Laboratories, it was demonstrated that the loss of TE_{01} propagating mode in a hollow metallic circular waveguide can be made significantly small [15]. Following that work, achieving a TE_{10} single-mode THz coupling and propagation up to 500 GHz in a metallic rectangular waveguide was accomplished [16], [17]. However, the TE_{10} operating mode, like all other TE and TM modes, is dispersive and presents a fundamental nature of cutoff frequency. This type of structure suffers from group velocity dispersion close to cutoff frequency, resulting in a non-recoverable distortion of ultra-fast pulse waveforms and dc-THz broadband signal transmission [18], [19]. Therefore, it has never been considered for the guiding of dc-to-high-frequency broadband signals or the transmission of pico-second digital pulses with all frequency components extending from dc to THz.

In 2001, promising studies reported and suggested a non-dispersive propagation of THz pulses through ultra-low ohmic loss TE_{10} mode in a parallel metal plate waveguide [20]. Additionally, a plasmonic mode in parallel metal plate waveguide was observed in which the field distribution of TEM mode is abruptly changed [21]. However, the diffraction loss in parallel metal plate waveguide is the dominant loss mechanism, and mitigating this diffraction loss is an impeding concern that must be addressed for any practical realization of such an ultra-low-loss THz waveguide [13], [14].

C. CONTRIBUTION OF THIS WORK

In this work, our recently proposed mode-selective transmission line (MSTL) [22]–[24] is studied and characterized in detail. Its physical characteristics, operation principle, and super-wideband propagation are further examined and discussed here. As its name implies, MSTL supports a dominant mode very similar to the case of the microstrip line quasi-TEM in the lower frequency range covering dc. It is then automatically reconfigured with the phenomenon of a mode conversion at higher-frequency (mmW in this case), and the fundamental mode becomes TE_{10} similar to the rectangular waveguide case, as explained in [22] and [23]. In this work, the mode coupling and mode conversion along MSTL are theoretically studied and mathematically formulated. A semi-analytical method of lines (MoL) [25], [26] is used to model and investigate the guided-wave properties of MSTL, including loss and dispersion characteristics, and to establish a systematic design approach for its applications. The structure is also simulated with numerical methods based on two different commercial software packages, namely finite element method of HFSS and finite integration technique of CST Microwave Studio, which are used to double-check the field distribution obtained by the MoL and to investigate the radiation loss. The structure is fabricated on two different substrates using two different fabrication processes. Design techniques, theoretical results, and simulated results are all verified by measurements.

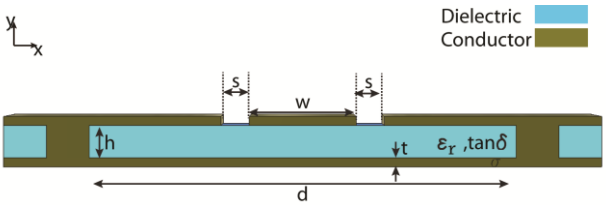

FIGURE 1. A cross section view of mode-selective transmission line.

II. MSTL STRUCTURE AND OPERATION PRINCIPLE

The cross-sectional view of a typical MSTL and its associated coordinate system for our analysis are shown in Fig. 1. The structure at first glance is similar to a dielectric-filled rectangular waveguide with two parallel slots etched on the top conductor layer, with a metal strip in the center. For the following modeling and analysis, the dielectric substrate of choice is characterized by dielectric constant ε_r, thickness h, and width d. The metallic layer has a large but finite conductivity σ, and the center metallic strip has width w and the slots of size s.

Fig. 2 shows the desired electric field distributions generated by numerical simulations in the cross section of MSTL. The two modes, supported by MSTL, have the electric field component aligned along the y-axis. Fig. 2(A) shows MSTL electric field at lower frequency and Fig. 2(B) shows MSTL electric field at higher frequency range. From dc up to cutoff frequency f_{cutoff} of TE_{10} mode of a rectangular waveguide of

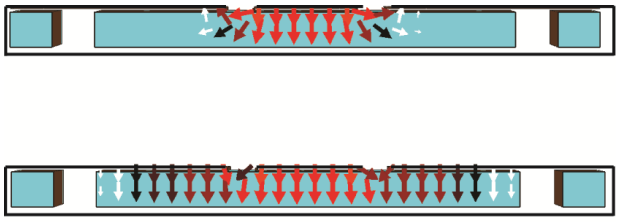

FIGURE 2. Intended modes in MSTL with the dominance of vertical electric field components: A) microstrip line mode, B) waveguide TE_{10} mode.

width d, the dimensions of MSTL are chosen in a way that the mode characteristic is very similar to the TEM mode of a microstrip line of strip width w. Cutoff frequency f_{cutoff} of TE_{10} mode is determined by:

$$f_{cutoff} = \frac{1}{2d\sqrt{\mu_0\varepsilon_0\varepsilon_r}} \tag{1}$$

At this frequency, attenuation constant of TE_{10} is large, and a strong mode coupling from the propagating TEM mode to TE_{10} mode takes place [22], [23], [27] and the electromagnetic power is transferred from one mode to another with the following interaction term:

$$P_{TE_{10},TEM} = \frac{1}{2}\oint\!\!\!\oint_S \overline{E}_{TE_{10}} \times \overline{H}^*_{TEM}.\widehat{a_z}ds \tag{2}$$

Since $\overline{E}_{TE} = E_y a_y$ and $\overline{H}_{TEM} = H_x a_x$, according to (2), the total coupling from TEM mode to TE_{10} mode is realized ($E_y a_y \times H_x a_x.a_z = E_y H_x a_y \times a_x.a_z = E_y H_x a_z.a_z = E_y H_x(a_z.a_z = 1)$).

Therefore, as frequency goes beyond the point of f_{cutoff}, mode characteristic becomes similar to the TE_{10} mode of rectangular waveguide or SIW [22], [23].

III. THEORETICAL DESCRIPTION

A. BACKGROUND

The common knowledge in our community is that mode conversion and coupling generally happen when there is a geometrical discontinuity or field disruption along the propagation direction [28]. This is absolutely true because the boundary condition is disrupted by the discontinuity. Interestingly, such mode conversion and coupling can also take place for a longitudinally uniform waveguide or transmission line as long as there is a presence of physical irregularities or field singularities within the cross section of the waveguide or transmission line in question. In this case, the formed mode is no longer a pure TEM mode or TE/TM mode, which cannot be describable by a closed-form analytical formulation. Indeed, such non-pure TEM or TE/TM modes can be regarded as a "coupled body" of pure mode (e.g., TEM mode) and the other modes. This mode coupling or energy conversion between the pure mode and other modes is enabled by dispersion as frequency changes (usually increases). This is because the guided mode is subject to the incremental adjustment of boundary condition

in which frequency definitely plays a role. Regarding the mathematical analysis, the mode conversion in an inhomogeneous cross section can be considered a problem of solving the Maxwell's equations with frequency-dependent boundary condition. The implication of dispersion effects in the formulation is implicit. Physically, single-waveguide mode coupling occurs [29] for which local modes are derived through wave optics or physical optics approximation [30].

B. MODE COUPLING AND MODE CONVERSION IN MSTL

MSTL is a longitudinally uniform guided-wave structure with an asymmetric inhomogeneous cross section. As frequency increases, the conversion of the zero-frequency propagation mode into an appropriate fundamental mode is necessary to satisfy the boundary condition. For the mathematical analysis, MSTL may be well considered as a multiconductor transmission line [31], namely a system of two coupled transmission lines:

1) Microstrip line of width w, and propagation constant β_1
2) SIW of width d, propagation constant β_2.

Both lines are made on the same substrate (ε_r, thickness h). Coupling characteristics between these two isolated transmission lines are expressed as a function of frequency. Below the cutoff frequency of SIW TE_{10} mode, f_{cutoff}, MSTL works as the microstrip line. Beyond frequency point f_{cutoff}, electromagnetic fields of the microstrip TEM mode and the SIW TE_{10} mode become overlapped and a mode coupling occurs between theses dissimilar integrated waveguides, which was briefly examined in one of our early works [34] but under different context. The key equations governing the mode coupling are reflected in overlap integral and coupling coefficient, which are obtained from the reciprocity theorem and defined for two coupled lines 1 and 2 by (3) and (4) [31]:

$$N_{12} = \frac{1}{2}\oint_S [E_1 \times H_2].a_z ds \tag{3}$$

$$Q_{12} = -\frac{j}{4}\int_{c_n} [E_{1,t}.J_{2,t} - E_{1,z}.J_{2,z}]dxdy \tag{4}$$

N_{12} determines the overlap between the two modes and Q_{12} resolves the coupling coefficient from the first mode to the other.

In this formulation, the eigenmode fields and currents of isolated microstrip line and isolated SIW are used (1: TEM and 2: TE_{10},). The field amplitudes are normalized so that $N_{11} = N_{22} = 1$ over all the frequency bands of interest and the coupling characteristics are derived:

$$N_{12} = \frac{2\sqrt{2}}{\pi}\sqrt{\frac{\Gamma}{\mu}}\sqrt{\frac{a}{w}}\sqrt{\frac{\beta_2}{\omega}}\sin(\frac{\pi w}{2a}) \tag{5}$$

$$N_{21} = \frac{2\sqrt{2}}{\pi}\sqrt{\frac{\mu}{\Gamma}}\sqrt{\frac{a}{w}}\sqrt{\frac{\omega}{\beta_2}}\sin(\frac{\pi w}{2a}) \tag{6}$$

$$Q_{12} = \sqrt{2\pi}\sqrt{\frac{\Gamma}{\mu}}\sqrt{\frac{1}{a^3 w}}\sqrt{\frac{1}{\omega\beta_2}} \tag{7}$$

(5) and (6) are the mode overlap integrals and (7) is the coupling coefficient from mode 1 to mode 2. The coupling coefficient from mode 2 to 1 $Q_{21} = 0$ because the current component of TEM mode is oriented only in the longitudinal z direction, whereas the longitudinal electric field of TE_{10} mode does not exist ($E_{z,TE10} = 0$). In the above equations, Γ is the free-space impedance, and $\omega = 2\pi f$. At the frequency at which the TE_{10} mode appears, ($\beta_2 > 0$), the coupling from TEM to TE_{10} is induced. Physically speaking, a mode conversion occurs where the propagation vector in the direction of inhomogeneity (k_x along the x-axis in this case) deviates [30]. Whereas for the TEM mode, the x-direction wavenumber is zero ($k_{x,TEM} = 0$), with the appearance of TE_{10} mode at f_{cutoff}, the value is changed to $k_{x,TE10} = \pi/a$. The mode conversion becomes strongest when their respective propagation constants are quite close to each other or equal [32].

As a result, for an input signal in this structure with frequency $f < f_{cutoff}$, a quasi-TEM mode dominates and for $f > f_{cutoff}$, a quasi-TE_{10} mode presides over, and therefore it is a mode-selective guided wave structure, enabled by a frequency change.

C. DISCUSSION

An assumption has always been made in the conventional modal analysis of a transmission line for which the modes are orthogonal to each other. This statement may be true if the modes belong to the same reference structure. However, in MSTL, the mode coupling takes place between two electrically different structures exhibiting different boundary conditions for those modes, which are no longer orthogonal in space. For the TEM mode, most of its electric field is confined under the center conductor, whereas for the TE_{10} mode, the electric fields are extended to the edges. With the electric fields of both modes being primarily vertical, none of the field components for the modes are orthogonal to each other. Therefore, the orthogonal coupled mode theory is no longer valid for the physical description of a mode-coupling process in this case.

Other forms of transmission lines, such as microstrip lines and coplanar waveguide, also support the frequency-dependent mode conversion and coupling phenomena caused by asymmetrical cross sections. However, in those structures, mode coupling and conversion result in strong dispersion and radiation. Such coupling effects are frequency-dependent and this is why some visible coupling effects can well be pronounced at high frequencies [33], [35]. Leaky-mode structures are a well-known example, as well as other examples in mutually-coupled hybrid mode structures, including complex mode issues [36], which are based on a uniform transmission line with an asymmetrical cross section; such an asymmetry does not need to be realized physically and it can even be managed electrically.

IV. DESIGN CONSIDERATIONS AND MSTL SIMULATION

Dimensions of MSTL should be adequately selected to ensure the expected mode conversion behavior over a desired frequency range. After choosing a substrate, width d is

TABLE 1. Electric and magnetic field distribution in the proposed MSTL on fused silica substrate at different frequencies: propagating modes change from TEM to TE_{10} mode.

Frequency	Field Distribution			
	E_y	H_x	H_z	
1GHz	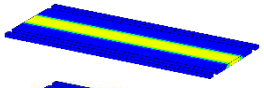	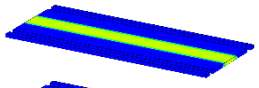	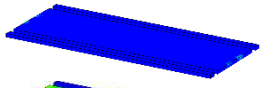	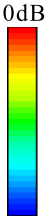
100GHz	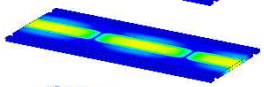	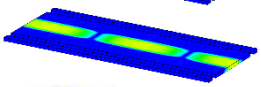	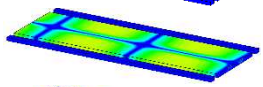	
300GHz	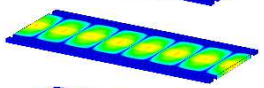	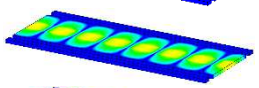	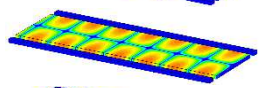	
500GHz	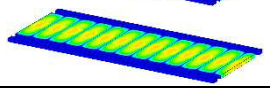	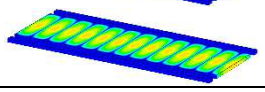	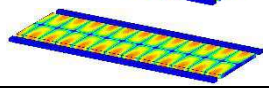	

selected as:

$$d > 8h \tag{8}$$

According to the potential theory for microstrip lines [37], the two conducting sidewalls have no influence on the characteristics of the microstrip line modal configuration in MSTL at low frequency operation, and fields and current distributions are very similar to the case of a quasi-TEM mode of standard microstrip line. Looking into (1), one can determine that width d also provides a direct control on the mode conversion frequency.

The possible presence of surface wave modes may deteriorate MSTL performance, especially along discontinuities. As such, considering the maximum operating frequency, thickness h must be thin enough to avoid the emergence of surface waves with the proposed design condition as follows [46]:

$$\frac{h}{\lambda_{\max}} < \frac{1}{2\sqrt{\varepsilon_r - 1}} \tag{9}$$

To avoid a potential excitation of the coplanar waveguide mode [38], dimensions w and s must be chosen with regard to the thickness in order to satisfy the following simple condition [22],

$$w/2 + s > h \tag{10}$$

In this work, single crystal fused silica (quartz) wafer (dielectric constant $\varepsilon_r = 4.27$ and $tan\delta = 0.0002$) with thickness $h = 50$ μm is selected as the prototype substrate to minimize the dielectric loss in the experiments. Width d is selected equal to 600 μm to have the frequency cutoff of TE_{10} mode around 120 GHz, and performing a parametric study (details will be given in the next section), the dimensions w and s are selected equal to $3h$ and $0.8h$, respectively. Finite integration technique numerical simulation of CST MWS is used for modeling MSTL through the calculation of its field distributions and mode conversion behavior. The results are shown in Table 1, from which the unique mode conversion propagation phenomenon is observed as anticipated. At relatively low frequencies, only transverse field components E_y and H_x exist, which are well confined to the center conductor, as expected for a TEM mode operation. By increasing frequency, the longitudinal magnetic field component H_z emerges, bouncing plane waves appear, and field distribution begins to extend toward the conductor sidewalls that makes up the quasi-TE_{10} mode.

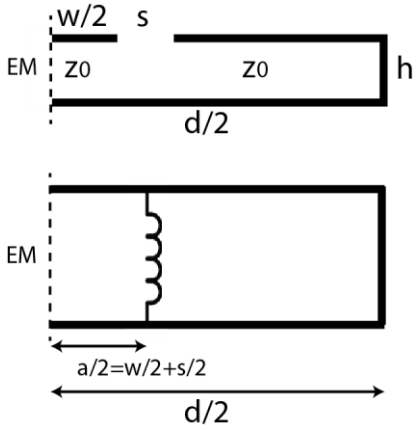

FIGURE 3. Equivalent transverse circuit network for MSTL in Fig. 1 with the reference plane in the middle of the slot s.

To be more accurate and also physically convincing, a possible effect of top metallic layer slits on f_{cutoff} of TE_{10} mode in MSTL, compared to SIW, as investigated in this work. Since $s/d \ll 1$ and substrate thickness h are less than the guided-wave wavelength, transverse resonance (TR) method [39] is deployed in this work to find the cutoff frequency of TE_{10} mode in MSTL. The equivalent transverse circuit network for the dominant operating mode consists of an inductance, representing non-radiating slits, shunted by two TE mode transmission lines with open- and short-circuit terminations. Fig. 3 shows the equivalent network modeling of the structure with the TR method in the TE-mode regime. The propagation

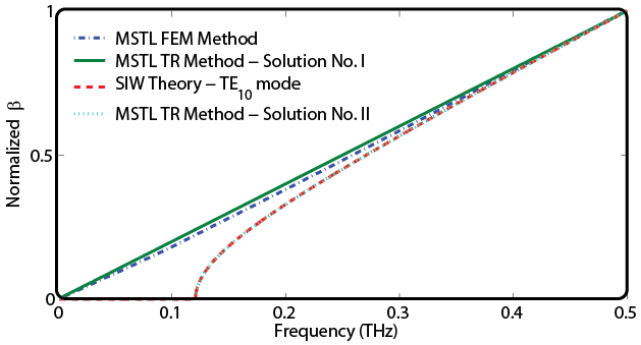

FIGURE 4. Propagation constant of guided-wave modes in MSTL using transverse resonance method and comparison with the results of FEM method and theoretical calculation [36].

constant is thus calculated from the following resonance condition:

$$\tan(\beta_x a/2) + \beta_x/Y_0 + \cot(\beta_x(d/2 - a/2)) = 0 \quad (11)$$

where

$$\beta_z = \sqrt{K^2 - \beta_x^2} \quad (12)$$

β_x is the transverse component of propagation constant, $Y_0 = 1/Z_0$ is the admittance of each part as shown in Fig. 3, and K is the wave number. The value of β_x/Y_0 is given by Marcuvitz in [39]. This equation leads to two solutions for the propagation constant, described in Fig. 4. To verify the results, the package of HFSS [40] is also used to simulate the proposed MSTL and calculate the propagation constant. As is seen, one of the TR method solutions, solution No. 1 in Fig. 4, shows a propagating mode with no cut-off frequency that has almost the same propagation constant as calculated by HFSS. The other solution, solution No. 2 in Fig. 4, shows a propagation constant almost the same as the TE_{10} mode of an SIW structure with the width d, having only 0.5% frequency shift toward the lower frequency side.

The HFSS simulated results are illustrated in Fig. 5. Fig. 5(A) shows the electric and magnetic field distributions of the proposed MSTL, and Figs. 5(B) and 5(C) present the propagation characteristics of the fundamental mode supported by MSTL and the comparison to the dispersion curve of the fundamental mode supported by microstrip line of width w, and rectangular waveguide of width d.

In the lower frequency range (I: dc to 120 GHz), the fields are confined to the proximity of the strip; both electric and magnetic fields, E_y and H_x with uniform distribution, lie in a perpendicular plane to the axis of propagation as one would expect for the TEM mode [27]. Over this frequency range, according to Figs. 5(B), and 5(C), phase constant and group velocity of the dominant mode are much the same as the TEM mode of microstrip line. As frequency approaches the cutoff of the TE_{10} mode, the magnetic field H_z appears and the power is converted from the quasi-TEM mode to a quasi-TE_{10} mode and the effective dielectric constant of the propagating mode is slightly increased [23]. Fig. 6 shows the calculated

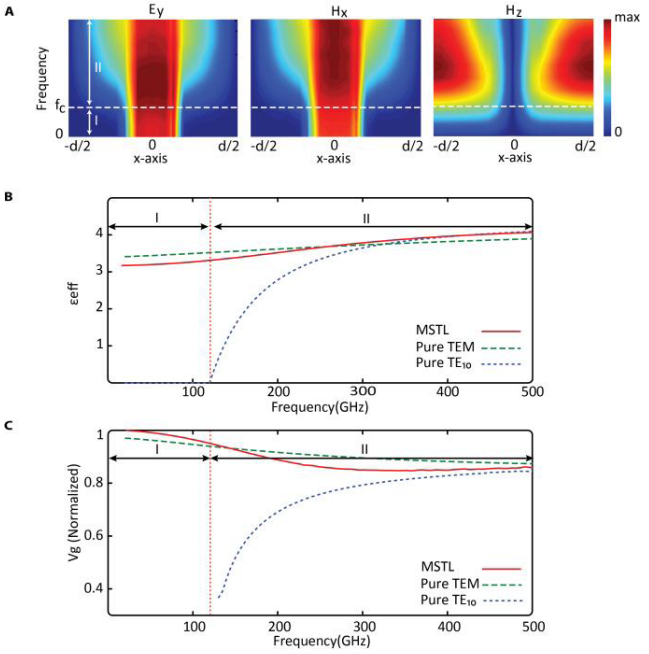

FIGURE 5. A) Fields and current distributions in MSTL designed on quartz (h=50μm, d=12h, w=3h, s=0.8h) from DC up to 0.5 THz range; f_c = 120GHz, f_{max} = 500GHz. In region I of frequency range, MSTL works under a mode with characteristics very similar to that of TEM mode. In region II, MSTL operates with a mode with characteristics very similar to TE_{10} mode. B) Effective dielectric constant of MSTL on quartz (h=50μm, d=12h, w=3h, s=0.8h) and comparison with effective dielectric constant of microstrip line TEM mode and rectangular waveguide TE10 mode. C) Group velocity of MSTL on quartz (h=50μm, d=12h, w=3h, s=0.8h) and comparison with group velocity of microstrip line TEM mode and rectangular waveguide TE_{10} mode.

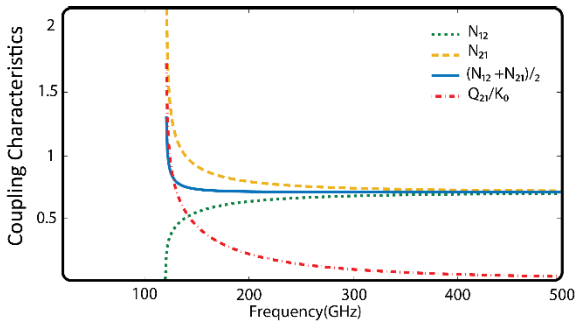

FIGURE 6. Calculated mode coupling characteristics for MSTL of fig. 5.

mode coupling characteristics using (10), (11), and (12). As it can be seen at the cutoff frequency f_{cutoff}, the overlap integral $(N_{12}+N_{21})/2$ and normalized coupling coefficient Q_{12}/K_0 are at their maximum values. MSTL shows a smooth effective dielectric constant transition over frequency, thus ensuring dispersion-less characteristics. This is because around that frequency range, hybrid TEM and TE_{10} modes exist.

V. MSTL WAVEGUIDING CHARACTERIZATION

The proposed MSTL is a planar waveguide that consists of regions that are homogenious in one direction. Therefore, a semi-analytical method of lines (MoL) is used in this work

for hybrid-mode analysis and evaluation of MSTL complex propagation constant $\gamma = j\beta + \alpha$, in which β is the phase constant and α is the attenuation constant [41], [42].

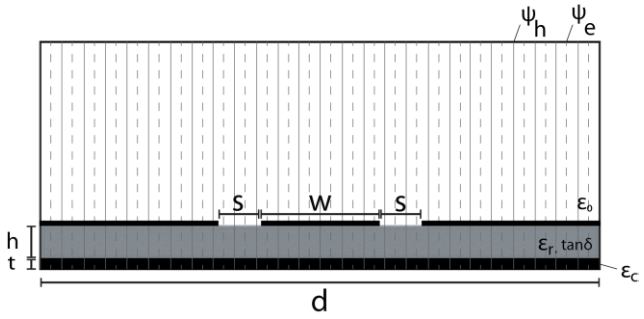

FIGURE 7. MSTL cross section with MOL discretization for hybrid-mode analysis.

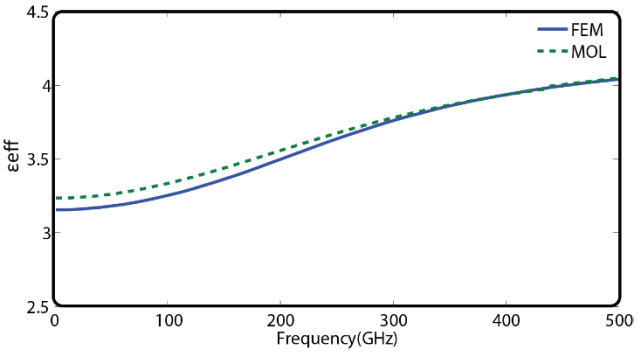

FIGURE 8. Comparison of calculated effective dielectric constant as a function of frequency using the MoL method and HFSS package; MSTL with geometrical parameters $\varepsilon_r = 4.27$, h=50μm, d=10h, w=3h, s=0.8h.

A. MODAL ANALYSIS

In the full-wave formulation of MoL, electric and magnetic potential functions are discretized along the x-direction (Fig. 7). Applying boundary conditions at the dielectric interface, the resulting Helmholtz equation in the discrete form is solved analytically after matrix transformation. Following a series of mathematical manipulations, a non-linear transcendental equation is obtained whose solutions lead to the eigenvalues associated with guided-wave characteristics. Therefore, effective dielectric constant is extracted over the whole frequency range from dc to 0.5 THz; electric field distribution is also derived and plotted on the cross section. To verify the accuracy and convergence of the discretization, the calculated effective dielectric constants are compared with the simulated finite element method results. Fig. 8 shows that the effective dielectric constant calculated with both methods demonstrates an excellent agreement in the high frequency range, and less than 3% difference in the low frequency region that may be caused by difference in discretization schemes.

B. LOSS DERIVATION

To determine exact sources of loss, the attenuation constant α is divided into metallic loss (α_c) stemming from the finite conductivity σ, and dielectric loss (α_d) related to the substrate loss, tangent $tan\delta$. Metallic loss includes the loss of both the bottom conductive layer (α_{c1}) and top metallic layer (α_{c2}). Therefore, attenuation constant is calculated from the total value with a linear superposition $\alpha = \alpha_d + \alpha_{c1} + \alpha_{c2}$ with reference to the principal of pertubation. The bottom electrode layer or groundplane is usually thicker than the strips on the substrate surface, and is regarded as a dielectric layer with a thickness t equal to skin effect [44]:

$$t = \sqrt{\frac{2}{\omega\mu\sigma}} \tag{13}$$

where $\omega = 2\pi f$ determines the angular frequency, and μ is the conductor permeability. This layer is modeled as a purely imaginary value with the permittivity ($\varepsilon_c = -j\frac{\sigma}{\omega}$) [45]. In the first step, a two-layer structure of dielectric substrate (ε_r, $tan\delta$) on the groundplane (ε_c) is modeled, and complex propagation constant $\gamma_1 = j\beta_1 + \alpha_1$ is obtained, in which the real part β_1 is the transmission line phase constant and the imaginary part includes the contribution of dielectric and lossy ground plane in the attenuation constant ($\alpha_d + \alpha_{c1}$). Subsequent to the calculation of β_1, field and current components are then calculated along the cross section of MSTL. In the second step, a perturbation method is used [46] to attenuation (α_{c2}), and finally the total loss (α) is derived. Radiation loss is not included in the above-mentioned MoL calculations, and it is estimated with the HFSS package. Fig. 9 shows the calculated loss from the specified different sources of loss and also the total loss in the MSTL. As it is seen from the MoL calculation, loss is mostly due to the top conductor layer. The mode conversion is perceptible from the curve trend; the guided-wave mode is changed from a semi-TEM mode to a semi-TE_{10} mode. The total loss is increased up to around 120 GHz, the TE_{10} mode cutoff frequency, and then decreased. After reaching a frequency point with minimum loss around 220 GHz, the loss rises again and continues steadily from around 400 GHz. The calculated radiation loss from the HFSS package is also added to Fig. 9, interestingly showing that the radiation loss vanishes after the mode conversion. It appears again at higher frequency that may be caused by slight slits radiation over that frequency range.

C. PARAMETRIC STUDY

In order to understand better the physical behavior of MSTL structure, and identify its limitations and design scheme, a comprehensive parametric study is performed in this section. Fig. 10(A) presents the effective dielectric constant ε_{eff} of MSTL for a variation of the center conductor width w. As is shown for constant thickness (h=*constant*) with decreasing w below $2h$, the occurrence of coplanar waveguide mode at higher frequency is observed. For example, when $w = 1.5h$, the coplanar waveguide mode begins to appear

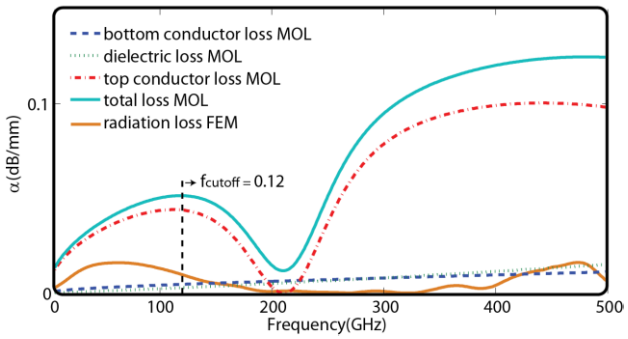

FIGURE 9. Calculated different sources of loss using the MoL, including radiation loss using the HFSS package (MSTL with parameters $\varepsilon_r = 4.27$, h=50μm, d=12h, w=3h, s=0.8h).

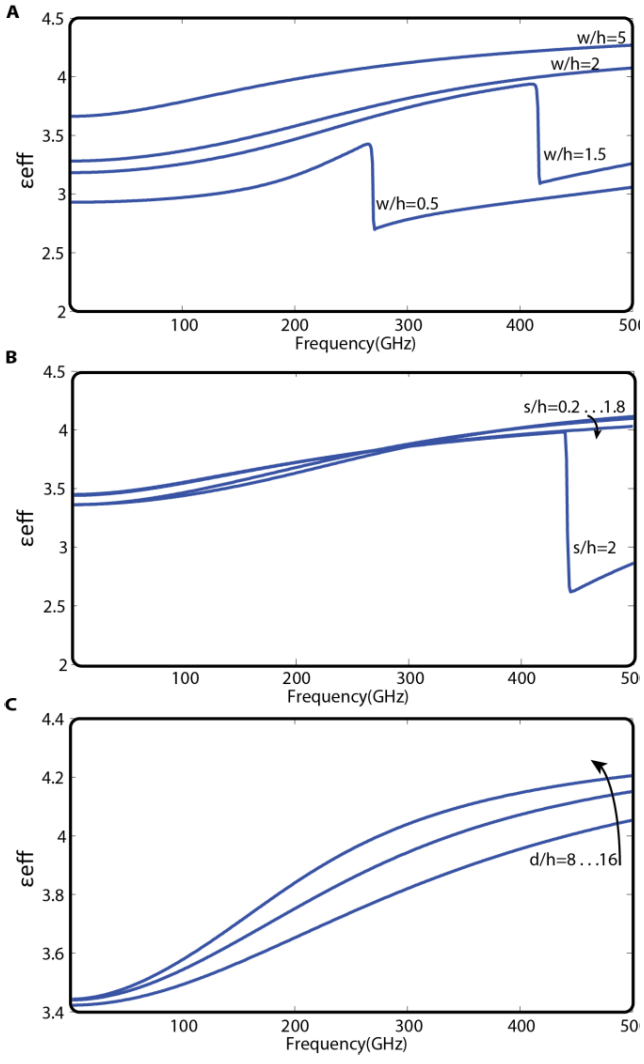

FIGURE 10. Computed effective dielectric constant as a function of frequency: A) Strip width w as a parameter, and $\varepsilon_r = 4.27$, h=50μm, d=12h, s=0.8h; B) Slot width s as parameter, and $\varepsilon_r = 4.27$, h=50μm, d=12h, w=3h; and C) Substrate width d as a parameter, and $\varepsilon_r = 4.27$, h=50μm, w=3h, s=0.8h.

around 420 GHz, and if $w = 0.5h$, it appears around 270 GHz. Fig. 10(B) plots the effective dielectric constant ε_{eff} of MSTL for a variation of slot width s. Again for constant thickness ($h = constant$) with increasing s above h, the occurrence of coplanar waveguide mode at higher frequency is observed. In this case, the upper limit for the parameter s is:

$$s < 1.8h \tag{14}$$

It is seen that if $s = 2h$, the coplanar waveguide mode starts to appear around 340 GHz. The lower limit of s is determined by the fabrication process. Fig. 10(C) shows the effect of width d on dispersion, and it can be seen that for constant h, a smaller d would result in a frequency-dependent response with lower dispersion.

The effect of waveguide width d on the loss is illustrated in Fig. 11. As it is clearly seen, at the cutoff frequency of TE_{10}, where the width d is greater than a half-wavelength, the mode conversion occurs, guided-wave power is transferred from semi-TEM mode to semi-TE_{10} mode, and loss is decreased. For constant thickness ($h = constant$) with increasing the value of d, the occurrence frequency of TE_{10} mode shifts to the lower frequency range.

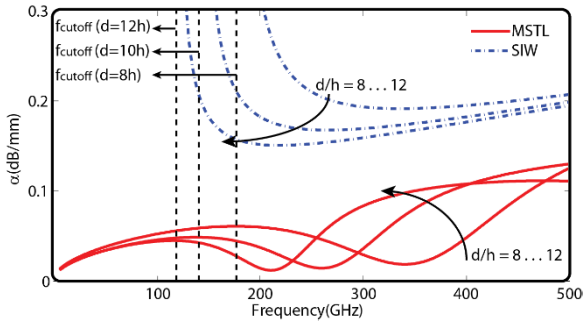

FIGURE 11. Comparison of calculated propagation loss of MSTL and SIW as a function of frequency for different waveguide width d, $\varepsilon_r = 4.27$, h=50μm, s=0.8h, w=3h.

In Fig. 11, the calculated conductor loss of MSTL is also compared to the calculated conductor loss of a dielectric-filled rectangular waveguide (SIW), with the same waveguide width, d, showing less attenuation in the case of MSTL. Conductor loss is in direct association with current distribution. Therefore, to clarify this observation, magnetic field and surface current vectors in SIW and MSTL are calculated and compared using HFSS full-wave analysis. Fig. 12 shows an example of this calculation at 250GHz in a waveguide of length L=1mm. The wave propagates along the waveguide where the bouncing plane waves of TE_{10} undergo a power loss at each bounce due to the imperfectly conducting surfaces [3]. In MSTL and SIW, the current distributions are similar, but MSTL presents a ''compressed TE_{10}'' mode due to the designed non-radiating slots on the top conductor. This compressed mode grants a lower conductor loss compared to a typical TE_{10} mode. The reason is that in MSTL compared to SIW, not only does the placement of the non-radiating slots not contribute to conductor loss, but also thanks to the TE_{10} compressed feature, the metallic sidewalls do not contribute to conductor loss and the structure dispersion becomes lower.

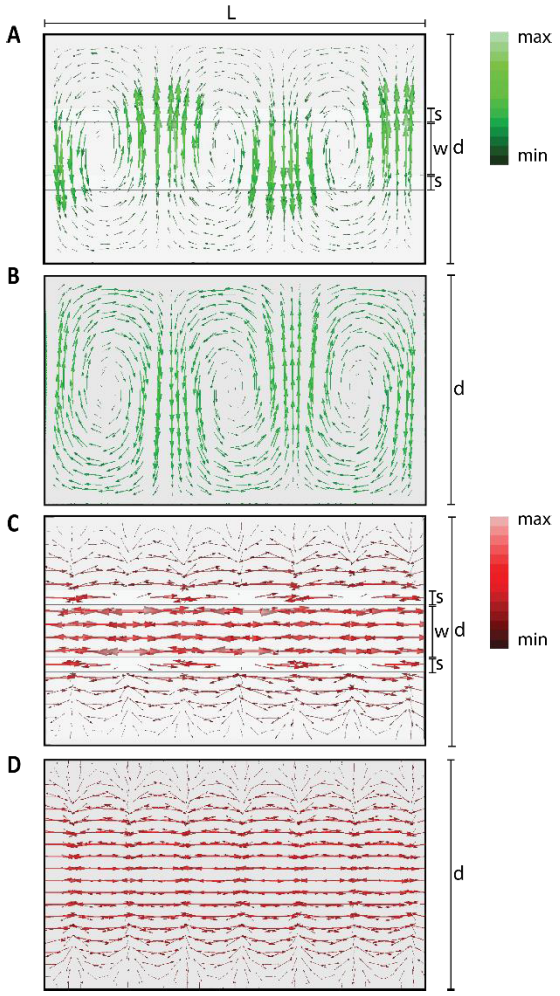

FIGURE 12. Magnetic field and current distribution at 250GHz: A) MSTL, Magnetic field B) SIW, Magnetic field C) MSTL, Surface current D) SIW, Surface current.

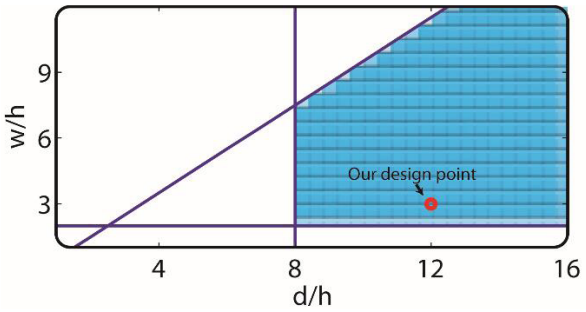

FIGURE 13. MSTL guiding design curves in w/h-d/h plane showing the useful design region of interest.

This explains why the proposed MSTL structure has a superior low-loss and low-dispersion performance.

The region of interest for MSTL design is defined by a set of values adapted to achieve a low-loss and low-dispersion characteristic in a desired bandwidth. The region of interest in the *d/h-w/h* plane is bounded by inequalities defined by (3) and (9), which define the minimum width of the waveguide and strip.

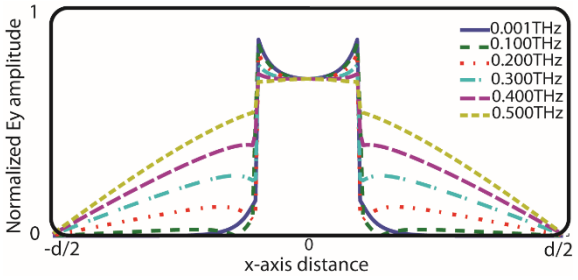

FIGURE 14. Ey distribution (along the x-direction) for the fundamental propagating mode in MSTL (ε_r = 4.27, h=50μm, d=12h, w=3h, s=0.8h).

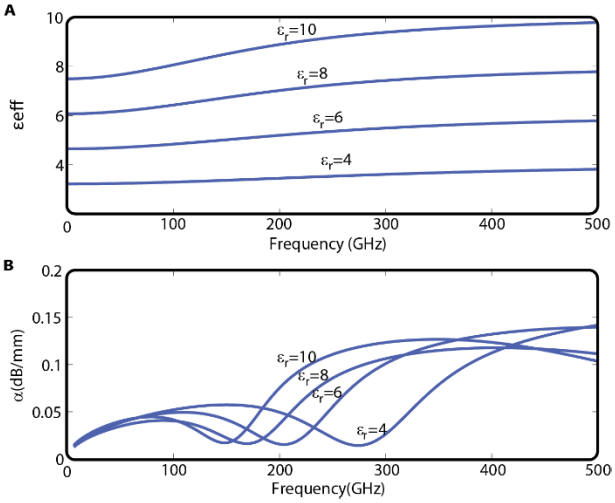

FIGURE 15. A) Calculated effective dielectric constant as a function of frequency with substrate permittivity ε_r as a changing parameter, and h=50μm, d=12h, w=3h, s=0.8h; B) Computed loss as a function of frequency with substrate permittivity ε_r as a changing parameter, and h=50μm, d=12h, w=3h, s=0.8h.

In addition, the cutoff of waveguide mode should be lower than the transverse resonance (TR) mode of microstrip line, which dictates [46]:

$$\frac{c}{2d\sqrt{\varepsilon_r}} < \frac{c}{\sqrt{\varepsilon_r}(2w+h)} \tag{15}$$

The defined design region is described in Fig. 13. Fig. 14 shows some typical field distributions from 1 to 500 GHz along the air-substrate interface ($y = h$), calculated through MoL. The field components are normalized to their amplitude at the strip center. Once again, the mode conversion is observed. As expected, the field is confined to the proximity of the strip over the low-frequency range. As frequency approaches the cut-off point of the first higher mode, the field is spread out up to the lateral boundaries. As frequency is raised from 1 GHz to 500 GHz, the field distributions are much changed from a pure microstrip mode to a quasi-sinusoidal distribution (waveguide mode). Therefore, it is empirically deduced that in the design process, the strip width w must also be smaller than half of the waveguide width d.

Fig. 15 depicts the effect of increasing dielectric substrate permittivity ε_r on the effective dielectric constant and

TABLE 2. Electric and magnetic field distribution in the proposed MSTL made on rogers substrate for different frequency points: propagating modes change from TEM mode to TE_{10} mode.

Frequency	Field Distribution		
	E_y	H_x	H_z
1GHz	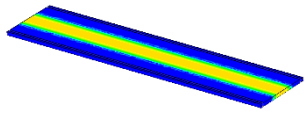	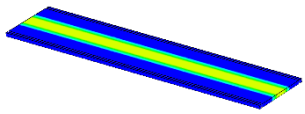	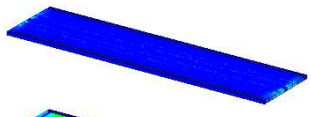
50GHz	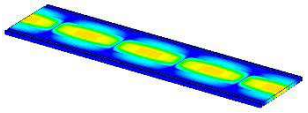	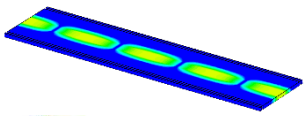	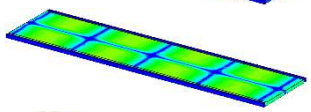
100GHz	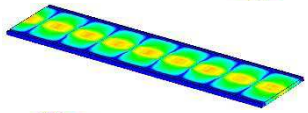	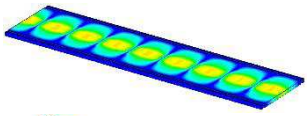	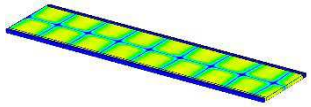
200GHz	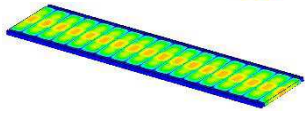	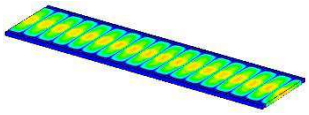	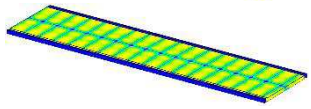
			0dB - 40dB

attenuation constant. ε_{eff} variation (dispersion) from low to high frequency increases with increasing ε_r, which can be expected as higher ε_r would contribute to a larger dispersion. The variation from 1 to 500 GHz is about 5% with $\varepsilon_r = 4$ and 20% with $\varepsilon_r = 10$. The effect of increasing the permittivity on dielectric loss tangent, and therefore the total loss, is negligible since the conductor losses are much larger than those from the dielectric substrate. The mode conversion frequency is decreased with increasing ε_r, where the curves are similar to the propagation loss variation as a function of waveguide width d, as shown in Fig .10.

VI. EXPERIMENTAL VERIFICATIONS

Our experimental prototypes of MSTL are fabricated through two different technological platforms. In addition to the fabrication of MSTL on a fused silica substrate, a PCB prototype is also designed based on the proposed design procedure using RT/duroid® 6002 laminates substrate from Rogers Corporation, with low dielectric constant $\varepsilon_r = 2.94$ and low loss substrate $tan\delta = 0.0012$, which is a proper choice for high frequency applications. Substrate thickness is chosen to be 127μm, which is the minimum available thickness of this substrate. Width d is selected equal to 1.5 mm ($\approx 12h$) making the conversion frequency around 60GHz. After a parametric study, w and s are selected equal to $2.4h$ and $1.6h$ for achieving minimum loss and dispersion. The CST package is used to calculate the field distribution and examine the mode conversion. Table 2 shows the simulation results in which the unique propagation phenomenon and the TEM-TE_{10} mode conversion are clearly spelled out. In the lower frequency range, transverse fields E_y and H_x are the only field components, and then longitudinal H_z emerges in the higher operating frequency. This evidence again confirms the mode selectivity over the frequency range.

A. FABRICATION

The fabrication of MSTL samples in our Poly-Grames Research Center on the fused silica wafer with 50 μm thickness presents some technical difficulties and challenges that have been addressed and briefed as follows. Since the substrate is very thin, a back coating metallization of the substrate with sputtering was done as the first step and the thin 50 μm quartz substrate was affixed to a thick 500 μm quartz substrate. Another major difficulty in the processing is related to its laser drilling, because quartz is optically transparent. Abrasive waterjet machining was used with a modified and refined head for drilling the side holes, as this tool is capable of cutting a wide variety of materials using a very high-pressure mixture of water and an abrasive substance. After filling up the holes and the final top sputtering, the patterning was made using a lithograph with less than 1 μm precision [23].

For the PCB prototype, the fabrication was done with an in-house standard printed circuit board (PCB) process with 1 mil precision and minimum 3 mil gap/trace combined with laser cutting to define the lateral walls.

B. MEASUREMENTS

On-wafer characterization was done with thru-reflect-line (TRL) calibration techniques to remove errors occurring during the measurements, and also to define the measurement reference planes. Picoprobes with ground-signal-ground (GSG) head were used in the measurements. To avoid forcing or exciting the unwanted coplanar waveguide mode in MSTL, the position between the middle of the center strip and the edges of the launch transition pads is calculated precisely. This avoids the propagation of coplanar waveguide mode and slot modes, prevents possible pad

parasitic capacitive effects, improves the placement accuracy of probe tips, and also minimizes mismatch. For the transition, slots are tapered out exponentially to the lateral boundaries and the center metal strip is tapered to the 50 Ω-impedance width. To guarantee a smooth transition between MSTL section and the microstrip line over a very wide frequency range, their characteristic impedance and field distributions are both matched. The transition provides a gradual transformation of electric fields from the microstrip mode to MSTL propagation mode. A quarter-wavelength multi-step profile of the strip provides the impedance matching. These steps are linearly shaped to vary gradually in geometry, resulting in a smooth field matching.

To test the MSTL, a PNA-X with millimeter-wave modules was used and TRL kits were designed for each 1:8 frequency band. For each millimeter-wave test module, a set of corresponding picoprobes is used. The PNA-X used in this work was limited to 750 GHz, but our available millimeter-wave test modules were limited to 500 GHz, and therefore the measurements are also limited to this frequency. Picoprobes' pitch dimensions decrease with increasing the frequency and above 110 GHz, which is less than the minimum tolerable PCB gap/trace in the processing of our laboratories. Therefore, in the case of the PCB-based MSTL prototype, the maximum frequency that we could measure was up to 110 GHz because of this PCB fabrication accuracy limitation.

A launch structure is required to interface between the GSG coplanar probe head and the MSTL. For the PCB prototype, large grounded via-holes were used as reflective sections. As operating frequency increases, its electrical length to the ground plane increases and the via-hole input impedance becomes inductive and prejudicial to the calibration and measurements. For the PCB prototype, oversized rectangular tranches are used to reduce the undesirable inductive effect. However, for the fused-silica prototype, a reflective section in the launch transition was designed with a radial quarter wavelength open sector. The use of such an open stub overcomes the undesirable reactive effects and avoids some fabrication uncertainties at higher frequency.

In the PCB prototype measurements from 10 MHz to 110 GHz, a 1-mm connector together with a 150-μm picoprobe was used, providing broadband and accurate outcomes [47]. For the measurements up to 500 GHz frequency probes, with a minimum pitch of 40 μm, were used. Our on-wafer measurements using high-frequency probes provide accurate and repeatable results. The millimeter-wave modules and their corresponding GSG pico-probes that were available for our measurement are based on rectangular waveguide and each of them is for a limited bandwidth. The measured bandwidth from DC to 500GHz is divided into 6 bands, for each band we use specific GSG pico-probes: fed by coaxial for (0 to 75GHz) range and by waveguides for the 5 other sub-bands namely: (WR10 (75-110 GHz), WR8 (90- 140 GHz), WR5 (140-200 GHz), WR3 (220- 325 GHz), WR 2(325-500 GHz)). Radial stub it primarily for providing a clean (no spurious resonances) broadband short circuit, much broader than a simple open-circuit stub. The radial stub cover more that 40% of bandwidth (at −20 dB of reflection) which is sufficient to cover each sub-bands.

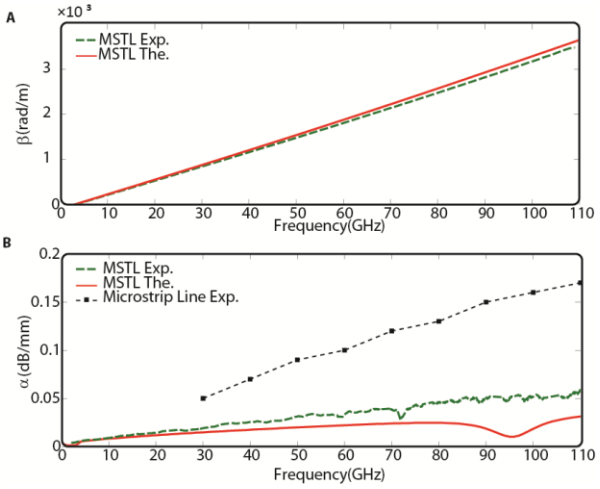

FIGURE 16. A) Comparison of theoretical and experimental propagation phase constant (β) of MSTL prototype fabricated on RT/duroid® 6002 laminates from Rogers Corp. (h=127um, d=20h, s=1.6h, w=2.4h), B) Comparison of theoretical and experimental propagation loss characteristics of MSTL prototype fabricated on RT/duroid® 6002 laminates from Rogers Corp. (h=127um, d=20h, s=1.6h, w=2.4h) and thin film microstrip line from ref [37].

Loss and propagation constants are extracted from the S-parameters. Fig. 16 shows PCB prototype measurement results and their comparison with the related MoL-calculated theoretical results. In Fig. 16(A), the loss of microstrip line on the same substrate, which has been reported by [47], is also shown. While MSTL shows loss less than 0.04 dB/mm over all the frequency ranges of interest, the loss of microstrip line reaches to 0.17 dB/mm at 110 GHz. Additionally, in the lower frequency range (TEM-mode frequency regime), a much lower loss is obtained for MSTL, which indicates a lower radiation loss compared to its corresponding microstrip line.

The transmission characteristics of the measured MSTL on the fused silica substrate up to 500 GHz are presented in Fig. 17. Fig. 17(A) shows the theoretical and experimental propagation phase constant over the entire frequency range of interest. Fig. 17(B) plots the theoretical and experimental attenuation of MSTL compared to the experimental result of a low dispersive thin-film microstrip line fabricated on low-resistivity Si with polymerized cyclotene as the high quality dielectric substrate from [40]. As expected, MSTL grants a continuous low attenuation characteristic over all the measured frequency range. The measured attenuation exhibits a frequency dependency; close to the TE_{10} cut-off frequency at 120 GHz, the attenuation falls off and goes up again to 200 GHz, from which it continues constantly and roughly flat over the frequency range of interest. However, in case of an optimized well-performing microstrip line, the attenuation easily increases with frequency up to 3dB/mm at 500 GHz [22], [23].

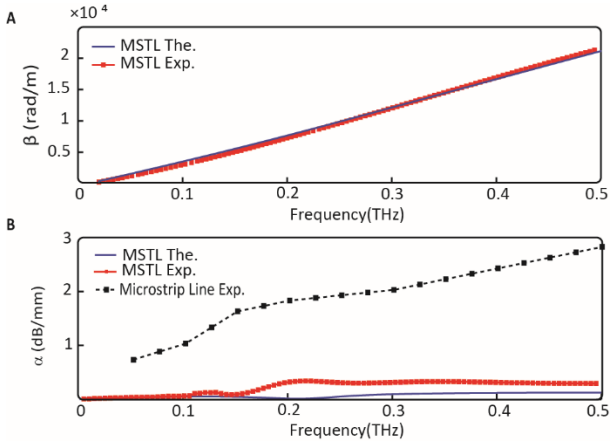

FIGURE 17. A) Comparison of theoretical and experimental propagation phase constant (β) of MSTL prototype fabricated on quartz (h=50um, d=12h, s=0.8h, w=3h); (B) Comparison of theoretical and experimental propagation loss characteristic of MSTL prototype fabricated on quartz (h=50um, d=12h, s=0.8h, w=3h) and thin film microstrip line from ref [39].

Except for some fabrication tolerances, other adverse factors may contribute to the discrepancy observed between the theoretical models and experimental measurements. Indeed, MSTL is subject to difficult-to-evaluate copper surface roughness effects in connection with current and field distributions. The field and current move more toward the bottom of the conductor surface, where a roughness lies. The copper surface roughness of substrate affects the conductor losses as well as the propagation constant of the transmission line [50]. Conductor trapezoidal effect or ''edge profile,'' where the conductors are considered to be rectangular, can increase the influence of copper surface roughness on loss and propagation constants. Morgan correlation [50] is a multiplicative correction factor K to the attenuation constant calculated for a smooth conductor, the RMS value of the conductor roughness, and the skin depth. At low frequencies where the skin depth is large, the value of K is close to one. With higher profile conductors and higher frequencies, the value of K approaches two. This correlation predicts that the maximum effect of the conductor roughness would be to double the conductor loss and saturate exactly as noticed in Figs. 15(B) and 16(B).

VII. CONCLUSIONS

The proposed MSTL, effectively covering from dc to THz frequency range with the desired operation, is found suitable for full-band electromagnetic propagation and ultra-high-speed pico-pulsed signal transmission. It can be made to support single-mode transmission over a super-wide range of frequency through the process of mode selectivity. Whereas at low frequency MSTL operates under the TEM-mode regime, the operating mode is gradually converted to a low-loss TE_{10} mode for operation at high frequency, such as mmW and THz. In this work, the MoL modeling technique together with two commercial software packages has been used in support of extensive theoretical modeling and numerical analysis dealing with field distributions and parametric studies. Careful experiments have been made with two different sets of experimental prototypes. Calculated, simulated and measured results are in good agreement, validating the proposed MSTL techniques. Physical mechanism and design approaches have been studied in detail. Low-loss and low-dispersion characteristics of MSTL have been well observed and explained with reference to the modal behavior and loss properties.

Through this research, the MSTL is found to allow for the possibility of developing densely integrated interconnects and planar guided-wave structures for dc-THz bandwidth applications. This concept points out a self-packaging solution that is necessarily required for THz and mmW integrated circuits. Combining the advantages of planar technology of low fabrication cost with the low-loss intrinsic to the operation mode, the MSTL is deemed to be a promising candidate for the future research and development of high-frequency performance-demanding integrated electronic and photonic circuits and systems in which broadband transmission lines are the most fundamental building elements and techniques, due to its unprecedented attractive features over the entire dc-THz electromagnetic spectrum.

REFERENCES

[1] S. Narenda, L. C. Fujino, and K. C. Smith, ''Through the looking glass continued (III): Update to trends in solid-state circuits and systems from ISSCC 2014 [ISSCC trends],'' *IEEE Solid-State Circuits Mag.*, vol. 6, no. 1, pp. 49–53, Jan. 2014.

[2] K. Feher, *Digital Communications*. Englewood Cliffs, NJ, USA: Prentice-Hall, 1981.

[3] J. Capmany and D. Novak, ''Microwave photonics combines two worlds,'' *Nature Photon.*, vol. 1, no. 6, pp. 319–330, 2007.

[4] F. Fesharaki and K. Wu, ''Band-pass non-TEM mode traveling-wave electro-optical polymer modulator for millimeter-wave and terahertz application,'' *J. Lightw. Technol.*, vol. 30, no. 23, pp. 3586–3596, Dec. 1, 2012.

[5] M. Tonouchi, ''Cutting-edge terahertz technology,'' *Nature Photon.*, vol. 1, no. 2, pp. 97–105, 2007.

[6] T. Kleine-Ostmann and T. Nagatsuma, ''A review on terahertz communications research,'' *J. Infr., Millim. Terahertz Waves*, vol. 32, no. 2, pp. 143–171, 2011.

[7] R. Saleh *et al.*, ''System-on-chip: Reuse and integration,'' *Proc. IEEE*, vol. 94, no. 6, pp. 1050–1069, Jun. 2006.

[8] K. Wu, ''Towards system-on-substrate approach for future millimeter-wave and photonic wireless applications,'' in *Proc. Asia–Pacific Microw. Conf.*, 2006, pp. 1895–1900.

[9] H. B. G. Casimir and J. Ubbink, ''The skin effect. I. Introduction the current distribution for various configurations,'' *Philips Tech. Rev.*, vol. 28, pp. 271–283, Jan. 1967.

[10] K. Wu, D. Deslandes, and Y. Cassivi, ''The substrate integrated circuits—A new concept for high-frequency electronics and optoelectronics,'' in *Proc. 6th Int. Conf. Telecommun. Modern Satellite, Cable, Broadcast. Service (TELSIKS)*, vol. 1. Nis, Yugoslavia, Oct. 2003, pp. P-III–P-X.

[11] M. Bozzi, A. Georgiadis, and K. Wu, ''Review of substrate-integrated waveguide circuits and antennas,'' *IET Microw., Antennas Propag.*, vol. 5, no. 8, pp. 909–920, 2011.

[12] F. Xu and K. Wu, ''Guided-wave and leakage characteristics of substrate integrated waveguide,'' *IEEE Trans. Microw. Theory Techn.*, vol. 53, no. 1, pp. 66–73, Jan. 2005.

[13] R. Mendis and D. M. Mittleman, ''An investigation of the lowest-order transverse-electric (TE_1) mode of the parallel-plate waveguide for THz pulse propagation,'' *J. Opt. Soc. Amer. B, Opt. Phys.*, vol. 26, no. 9, pp. A6–A13, 2009.

[14] R. Mendis and D. M. Mittleman, "Comparison of the lowest-order transverse-electric (TE_1) and transverse-magnetic (TEM) modes of the parallel-plate waveguide for terahertz pulse applications," *Opt. Exp.*, vol. 17, no. 17, pp. 14839–14850, 2009.

[15] E. A. J. Marcatili and R. A. Schmeltzer, "Hollow metallic and dielectric waveguides for long distance optical transmission and lasers," *Bell Syst. Tech. J.*, vol. 43, pp. 1783–1809, Jul. 1964.

[16] G. Gallot, S. P. Jamison, R. W. McGowan, and D. Grischkowsky, "Terahertz waveguides," *J. Opt. Soc. Amer. B, Opt. Phys.*, vol. 17, no. 5, pp. 851–863, May 2000.

[17] R. Mendis and D. Grischkowsky, "THz interconnect with low-loss and low-group velocity dispersion," *IEEE Microw. Wireless Compon. Lett.*, vol. 11, no. 11, pp. 444–446, Nov. 2001.

[18] S. Coleman and D. Grischkowsky, "A THz transverse electromagnetic mode two-dimensional interconnect layer incorporating quasi-optics," *Appl. Phys. Lett.*, vol. 83, no. 18, pp. 3656–3658, 2003.

[19] S. Coleman and D. Grischkowsky, "Parallel plate THz transmitter," *Appl. Phys. Lett.*, vol. 84, no. 5, pp. 654–656, 2004.

[20] R. Mendis and D. Grischkowsky, "Undistorted guided-wave propagation of subpicosecond terahertz pulses," *Opt. Lett.*, vol. 26, no. 11, pp. 846–848, 2001.

[21] J. Liu, R. Mendis, and D. M. Mittleman, "The transition from a TEM-like mode to a plasmonic mode in parallel-plate waveguides," *Appl. Phys. Lett.*, vol. 98, no. 23, p. 231113, 2011.

[22] F. Fesharaki, T. Djerafi, M. Chaker, and K. Wu, "Low-loss and low-dispersion transmission line over DC-to-THz spectrum," *IEEE Trans. THz Sci. Technol.*, vol. 6, no. 4, pp. 611–618, Jul. 2016.

[23] F. Fesharaki, T. Djerafi, M. Chaker, and K. Wu, "Mode-selective transmission line for DC-to-THz super-broadband operation," in *IEEE MTT-S Int. Microw. Symp. Dig.*, May 2016, pp. 1–4.

[24] F. Fesharaki, T. Djerafi, M. Chaker, and K. Wu, "High-integrity terabit-per-second signal interconnects with mode-selective transmission line," in *IEEE MTT-S Int. Microw. Symp. Dig.*, May 2016, pp. 1–4.

[25] U. Schulz and R. Pregla, "A new technique for the analysis of the dispersion characteristics of planar waveguides and its application to microstrips with tuning septums," *Radio Sci.*, vol. 16, no. 6, pp. 1173–1178, 1981.

[26] S. B. Worm and R. Pregla, "Hybrid-mode analysis of arbitrarily shaped planar microwave structures by the method of lines," *IEEE Trans. Microw. Theory Techn.*, vol. 32, no. 2, pp. 191–196, Feb. 1984.

[27] R. E. Collin, *Field Theory of Guided Waves*. New York, NY, USA: McGraw-Hill, 1960, chs. 4–5.

[28] C. C. Tang, *Advances in Microwaves*, vol. 4. New York, NY, USA: Academic, 1969.

[29] J.-M. Liu, *Photonic Devices*. Cambridge, U.K.: Cambridge Univ. Press, 2009, ch. 4.

[30] C. A. Balanis, *Advanced Engineering Electromagnetics*. Hoboken, NJ, USA: Wiley, 1989, ch. 7.

[31] K. Yasumoto, "Coupled-mode formulation of multilayered and multiconductor transmission lines," *IEEE Trans. Microw. Theory Techn.*, vol. 44, no. 4, pp. 585–590, Apr. 1996.

[32] M. N. Rosenbluth and R. Z. Sagdeev, *Handbook of Plasma Physics*. Amsterdam, The Netherlands: North-Holland, 1983, ch. 24.

[33] Z. Ma, E. Yamashita, and S. Xu, "Hybrid-mode analysis of planar transmission lines with arbitrary metallization cross sections," *IEEE Trans. Microw. Theory Techn.*, vol. 41, no. 3, pp. 491–497, Mar. 1993.

[34] A. Patrovsky, M. Daigle, and K. Wu, "Coupling mechanism in hybrid SIW–CPW forward couplers for millimeter-wave substrate integrated circuits," *IEEE Trans. Microw. Theory Techn.*, vol. 56, no. 11, pp. 2594–2601, Nov. 2008.

[35] C.-C. Tien, C.-K. C. Tzuang, S. T. Peng, and C.-C. Chang, "Transmission characteristics of finite-width conductor-backed coplanar waveguide," *IEEE Trans. Microw. Theory Techn.*, vol. 41, no. 9, pp. 1616–1624, Sep. 1993.

[36] P. Lampariello, F. Frezza, and A. A. Oliner, "The transition region between bound-wave and leaky-wave ranges for a partially dielectric-loaded open guiding structure," *IEEE Trans. Microw. Theory Techn.*, vol. 38, no. 12, pp. 1831–1836, Dec. 1990.

[37] B. E. Kretch and R. E. Collin, "Microstrip dispersion including anisotropic substrates," *IEEE Trans. Microw. Theory Techn.*, vol. 35, no. 8, pp. 710–718, Aug. 1987.

[38] G. Ghione and C. U. Naldi, "Coplanar waveguides for MMIC applications: Effect of upper shielding, conductor backing, finite-extent ground planes, and line-to-line coupling," *IEEE Trans. Microw. Theory Techn.*, vol. 35, no. 3, pp. 260–267, Mar. 1987.

[39] N. Marcuvitz, *Waveguide Handbook*, vol. 10. New York, NY, USA: McGraw-Hill, 1951.

[40] J. A. Deibel, M. Escarra, N. Berndsen, K. Wang, and D. M. Mittleman, "Finite-element method simulations of guided wave phenomena at terahertz frequencies," *Proc. IEEE*, vol. 95, no. 8, pp. 1624–1640, Aug. 2007.

[41] U. Schulz and R. Pregla, "A new technique for the analysis of the dispersion characteristics of planar waveguides," *Arch. Elektronik Uebertragungstechnik*, vol. 34, pp. 169–173, Apr. 1980.

[42] U. Schulz and R. Pregla, "A new technique for the analysis of the dispersion characteristics of planar waveguides and its application to microstrips with tuning septums," *Radio Sci.*, vol. 16, no. 6, pp. 1173–1178, 1981.

[43] S. B. Worm and R. Pregla, "Hybrid-mode analysis of arbitrarily shaped planar microwave structures by the method of lines," *IEEE Trans. Microw. Theory Techn.*, vol. 32, no. 2, pp. 191–196, Feb. 1984.

[44] K. Wu and R. Vahldieck, "Field distribution and dispersion characteristics of fundamental and higher-order modes in miniature hybrid MIC (MHMIC) considering finite conductor thickness and conductivity," in *IEEE MTT-S Int. Microw. Symp. Dig.*, Jul. 1991, pp. 995–998.

[45] F. J. Schmückle and R. Pregla, "The method of lines for the analysis of lossy planar waveguides," *IEEE Trans. Microw. Theory Techn.*, vol. 38, no. 10, pp. 1473–1479, Oct. 1990.

[46] D. M. Pozar, *Microwave Engineering*, 4th ed. New York, NY, USA: Wiley, 2009, ch. 3.

[47] K. Howell and K. Wong, "DC to 110 GHz measurements in coax using the 1 mm connector," *Microw. J.*, vol. 42, no. 7, pp. 22–34, 1999.

[48] D. C. Thompson, O. Tantot, H. Jallageas, G. E. Ponchak, M. M. Tentzeris, and J. Papapolymerou, "Characterization of liquid crystal polymer (LCP) material and transmission lines on LCP substrates from 30 to 110 GHz," *IEEE Trans. Microw. Theory Techn.*, vol. 52, no. 4, pp. 1343–1352, Apr. 2004.

[49] H.-M. Heiliger *et al.*, "Low-dispersion thin-film microstrip lines with cyclotene (benzocyclobutene) as dielectric medium," *Appl. Phys. Lett.*, vol. 70, no. 17, pp. 2233–2235, 1997.

[50] S. P. Morgan, Jr., "Effect of surface roughness on eddy current losses at microwave frequencies," *J. Appl. Phys.*, vol. 20, no. 4, pp. 352–362, 1949.

FAEZEH FESHARAKI received the B.Sc. degree in electrical and computer engineering from the Isfahan University of Technology, Iran, in 2008, and the M.A.Sc. (Hons.) and Ph.D. degrees in electrical and computer engineering from Ecole Polytechnique, University of Montreal, Canada, in 2011 and 2016, respectively. She was the recipient prestigious FRQNT and NSERC PDF award and she continued her research activities at the Optical Systems and Technology Laboratory, University of Victoria, BC, Canada. Her research interests include dc to terahertz (THz) integrated circuits, THz transceiver, high-speed electro-optic devices, millimeter-wave, and THz photonic.

TAREK DJERAFI (M'12) received the B.Sc. degree from the Institut d'Aeronautique de Blida, Blida, Algeria, in 1998, and the M.A.Sc. and Ph.D. degrees (Hons.) in electrical engineering from the École Polytechnique de Montréal, Montréal, QC, Canada, in 2005 and 2011, respectively. He was with SCP SCIENCE, Montréal, as an EMC Expert, from 2010 to 2011, a Post-Doctoral Fellow with Institut National de Recherche Scientifique, Énergie Matériaux et Télécommunications (INRS-EMT), Montréal, from 2012 to 2014, and École Polytechnique de Montréal from 2014 to 2015. He was a Research Associate with the Poly-Grames Research Center, Montréal, from 2015 to 2016. He is currently an Assistant Professor with INRS-EMT. His current research interests include the telecommunication antennas, beam formingnetwork, and RF/millimeter-wave/terahertz components and systems design.

MOHAMED CHAKER has been a Professor with INRS-EMT since 1989. He is currently the Director of the Laboratory of Micro and Nanofabrication. He has been holding a Canada Research Chair in plasmas applied to micro and nanomanufacturing technologies since 2003. He has authored over 250 articles in peer-reviewed journals in various domains, including advanced plasma sources characterization (high-density plasmas and laser-induced plasmas) for applications to thin-film synthesis, nanometer etching, nanoparticles production, and device fabrication. He is also the Co-Chair of the International Laboratory in Plasma Science and Technologies.

KE WU (M'87–SM'92–F'01) received the B.Sc. degree (Hons.) in radio engineering from Southeast University, China, in 1982, and the D.E.A. and Ph.D. degrees (Hons.) in optics, optoelectronics, and microwave engineering from the Institut National Polytechnique de Grenoble and the University of Grenoble, France, in 1984 and 1987, respectively.

He was the Founding Director of the Center for Radiofrequency Electronics Research of Quebec (Regroupement stratégique of FRQNT) and the Tier-I Canada Research Chair in RF and millimeter-wave engineering. He has also held guest, visiting, and honorary professorships with many universities around the world. He has been the Director of the Poly-Grames Research Center. He is currently a Professor of Electrical Engineering and the NSERC-Huawei Industrial Research Chair in future wireless technologies with the Polytechnique Montréal (University of Montreal), QC, Canada. He has authored or co-authored over 1100 referred papers and a number of books/book chapters. He has filed over 40 patents. His current research interests involve substrate integrated circuits, antenna arrays, advanced computer-aided design and modeling techniques, non-linear wireless technologies, wireless power transmission and harvesting, and development of RF and millimeter-wave transceivers and sensors for wireless systems and biomedical applications. He is also interested in the modeling and design of microwave and terahertz photonic circuits and systems.

Dr. Wu is a fellow of the Canadian Academy of Engineering and the Royal Society of Canada (The Canadian Academy of the Sciences and Humanities). He is a member of Electromagnetics Academy, Sigma Xi, and URSI. He was an IEEE MTT-S Distinguished Microwave Lecturer from 2009 to 2011. He is the 2016 IEEE MTT-S President. He is the Inaugural Three-Year Representative of North America as a Member of the European Microwave Association General Assembly. He was a recipient of many awards and prizes, including the first IEEE MTT-S Outstanding Young Engineer Award, the 2004 Fessenden Medal of the IEEE Canada, the 2009 Thomas W. Eadie Medal of the Royal Society of Canada, the Queen Elizabeth II Diamond Jubilee Medal in 2013, the 2013 FCCP Education Foundation Award of Merit, the 2014 IEEE MTT-S Microwave Application Award, the 2014 Marie-Victorin Prize (Prix du Quebec - the highest distinction of Québec in the natural sciences and engineering), the 2015 Prix d'Excellence en Recherche et Innovation of Polytechnique Montréal, and the 2015 IEEE Montreal Section Gold Medal of Achievement. He has held key positions in and has served on various panels and international committees, including the Chair of Technical Program Committees, International Steering Committees, and international conferences/symposia. In particular, he was the General Chair of the 2012 IEEE Microwave Theory and Techniques (IEEE MTT-S) International Microwave Symposium. He was the Chair of the joint IEEE chapters of MTT-S/AP-S/LEOS, Montreal, QC, Canada. He is currently the Chair of the newly restructured IEEE MTT-S Montreal Chapter. He is an elected IEEE MTT-S Administrative Committee (AdCom) Member from 2006 to 2015 and has served as the Chair of the IEEE MTT-S Transnational Committee, Member and Geographic Activities Committee, and Technical Coordinating Committee among many other AdCom functions. He has served on the Editorial/Review Boards of many technical journals, transactions, proceedings, and letters and scientific encyclopedia, including as an Editor or a Guest Editor.